

Microfluidic QCSK Transmitter and Receiver Design for Molecular Communication

Dadi Bi, *Student Member, IEEE*, Yansha Deng, *Member, IEEE*

Abstract—The components with molecular communication (MC) functionalities can bring an opportunity for emerging applications in fields from personal healthcare to modern industry. In this paper, we propose the designs of the microfluidic transmitter and receiver with quadruple concentration shift keying (QCSK) modulation and demodulation functionalities. To do so, we first present an AND gate design, and then apply it to the QCSK transmitter and receiver design. The QCSK transmitter is capable of modulating two input signals to four different concentration levels, and the QCSK receiver can demodulate a received signal to two outputs. More importantly, we also establish a mathematical framework to theoretically characterize our proposed microfluidic circuits. Based on this, we first derive the output concentration distribution of our proposed AND gate design, and provide the insight into the selection of design parameters to ensure an exhibition of desired behavior. We further derive the output concentration distributions of the QCSK transmitter and receiver. Simulation results obtained in COMSOL Multiphysics not only show the desired behavior of all the proposed microfluidic circuits, but also demonstrate the accuracy of the proposed mathematical framework.

Index Terms—AND gate, chemical reactions, microfluidics, molecular communication, QCSK modulation and demodulation, signal processing.

I. INTRODUCTION

Over the past few years, molecular communication (MC) has attracted increasing attention as it can wave revolutionary and interdisciplinary applications ranging from healthcare, to industry, and military [2], [3]. The wide range of applications inspired a bulk of research centering around theoretical characterizations of MC, such as transmission schemes [4], [5], propagation characterizations [6], [7], reception models [8], [9], and detection strategies [10], [11]. To ensure successful information transmission, signal processing units are essential components for MC transmitter and receiver to facilitate modulation-demodulation and encoding-decoding functionalities. However, how to practically realize these basic signal processing functions in microscale/nanoscale has been rarely studied.

The signal processing functions realized in existing MC works were performed over electrical signals using electronic devices. In [5], [12]–[15], the transmitted bit sequence was modulated over the concentration of signaling molecules via the on/off of an air tank [5], [12], [13], electronic spray [14],

and light-emitting diode (LED) controlled by Arduino microcontroller boards and laptops [15]. Their high dependency on electrical signals/devices can hardly fulfill the biocompatible and non-invasive requirements of biomedical applications, such as disease diagnosis and drug delivery [16]. Meanwhile, the size of electronic devices can hardly meet the requirement of intra-body healthcare applications promised by MC, where fully MC functional devices are expected to be miniaturized into microscale/nanoscale [2].

In nature, signal processing functions can be realized in molecular domain by exploiting a gene expression process, where transcription factors bind with genes to either activate or repress their expression into proteins [17]. If the transcription factor activates protein expression, the gene expression process can function as a buffer gate [18]. On the contrary, if the transcription factor represses protein expression, the gene expression process can function as a NOT gate [19]. The signal processing nature of gene expression process motivates biologists to design more complex artificial genetic circuits to manipulate molecular concentrations using synthetic biology [20]. One type of artificial genetic circuit with computing functions is the Boolean inspired digital logic device. The sharp state change between a low concentration and a high concentration is ideal for reliable state transitions and signal integration, making digital logic particularly useful in decision-making circuits [21]. For example, the authors of [19] designed an orthogonal AND gate and coupled it to nonspecific sensors to increase selectivity [22]. The authors of [23] constructed a simple NOR logic gate and spatially configured multiple NOR gates to produce all possible two-input gates, which have found their utilities in biotechnological applications [24].

Although the aforementioned genetic circuits have advantages in biocompatibility and miniaturization over electric circuits, the experimental realization of genetic circuits faces challenges, such as slow speed, unreliability, and non-scalability [25]. These challenges motivate our initial work on chemical reactions-based microfluidic circuits [26]–[28]. Unlike genetic circuits, chemical circuits are much easier to be controlled. Moreover, the integration of chemical reactions with microfluidic systems not only endows chemical circuits with advantages of rapid analysis and low reagent costs due to a reduction of circuit size [29], but can also benefit from an additional space level of chemical control through applying and regulating chemical reactions in different regions of a microfluidic device. In [26], [27], we designed an MC microfluidic transceiver based on chemical reactions to successfully realize binary concentration shift keying (BCSK)

Manuscript received September 29, 2021; revised March 24, 2022; accepted July 4, 2022. D. Bi and Y. Deng are with the Department of Engineering, King's College London, London, WC2R 2LS, U.K. (e-mail: {dadi.bi, yansha.deng}@kcl.ac.uk). (Corresponding author: Yansha Deng). This paper was presented in part at the ACM International Conference on Nanoscale Computing and Communication Conference, Virtual, September 2020 [1]. This work was supported by the Engineering and Physical Sciences Research Council (EPSRC), U.K., under Grant EP/T000937/1.

modulation and demodulation functions. The signal processing capability of chemical reactions-based microfluidic circuits was further exploited in [28], where we provided the designs of AND, NAND, OR, NOR, and XOR gates. These logic computation units can be applied to environmental monitoring. For example, the AND microfluidic circuit can improve the selectivity of a biosensor by producing a measurable signal only in the presence of multiple chemical signals. As we discussed in [28], one challenge in realizing signal processing functions via chemical reactions-based microfluidic circuits is the theoretical characterization of a logic gate, which facilitates the selection of design parameters for expected gate outputs. Although we mathematically modeled the dynamics of molecular species in microfluidic channels in [26], [27], this analysis is not scalable with the increase in the number of microfluidic circuits. Motivated by above, the objective of this paper is to employ microfluidic logic gates to achieve QCSK modulation-demodulation function and establish a mathematical framework to analyze any microfluidic MC circuit. The main contributions of this paper are as follows:

- We first present a chemical reactions-based microfluidic AND gate design, based on which, we design the microfluidic transmitter and receiver with quadruple concentration shift keying (QCSK) modulation and demodulation functionalities, to show how logic computations can process molecular concentrations and realize communication functionalities. The QCSK transceiver design largely expands the brief investigation of the digital signal processing capability of microfluidic circuits in [1]. Most importantly, we show how digital electronics theory can be applied to and facilitate microfluidic circuit design, which serves as a foundation for utilizing simple microfluidic logic gates to achieve more complex MC functions.
- We develop a novel mathematical framework to characterize our proposed microfluidic circuits, which can be applied to analyze other new and more complicated microfluidic circuits. As in [1], we first analyze the concentration and velocity changes under fluid mixing, but in this work we also consider the fluid separation scenario. Then we derive the impulse response of a straight convection-diffusion channel. Based on these, we derive the spatial-temporal concentration distribution of a convection-diffusion-reaction channel with either a thresholding reaction or an amplifying reaction.
- To evaluate our proposed microfluidic designs, we identify four elementary microfluidic blocks of the basic AND gate, and define five corresponding operators to represent the output concentration distribution of each elementary block. Relying on these, we derive not only the output concentration distribution of the proposed AND gate, but also the output distributions for our designed QCSK transmitter and receiver. The functionalities of our proposed microfluidic designs and the corresponding theoretical results are validated via simulations performed in COMSOL Multiphysics finite element solver.

The remainder of this paper is organized as follows. In Sec.

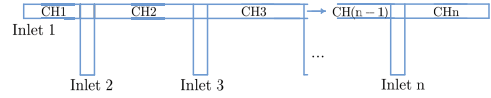


Fig. 1. A microfluidic device for fluid mixing analysis.

II, we provide the basic microfluidic channel analysis. In Sec. III, we establish a mathematical framework to theoretically characterize our proposed AND gate. In Sec. IV, we propose the designs and analysis of the QCSK transmitter and receiver. Numerical results in Sec. V validate the proposed microfluidic designs and their theoretical analyses. Finally, Sec. VI concludes the paper.

II. BASIC MICROFLUIDIC CHANNEL ANALYSIS

With the ultimate goal of designing and analyzing a microfluidic system with modulation and demodulation functionalities, the basic characteristics of fluids in microfluidic channels must be first understood. To do so, we analyze and derive the concentration and velocity changes for a general microfluidic device with combining channels (Sec. II-A) and separation channels (Sec. II-B), which are not fully investigated in the existing literature. We present the new results as lemmas in order to distinguish them from the known results in fluid dynamics. In particular, these lemmas hold under the assumption that the flow is laminar, viscous, and incompressible. The results provided in this section serve as the foundation for the analysis in the following sections.

For a Poiseuille flow traveling along the x direction of a microfluidic channel with rectangular cross-section, the average velocity can be expressed in terms of volumetric flow rate Q and cross-sectional area as [30, eq. (5)]

$$v_{\text{eff}} = Q/wh, \quad (1)$$

where w and h are the width and the height of the cross-section.

A. Fluid Mixing at Combining Connections

In a microfluidic circuit, fluids flowing in different channels can mix to a single flow at a combining connection, and we name this behavior as fluid mixing for simplicity.

1) *Concentration Change*: Let us consider a microfluidic device with n inlets and n combining channels as shown in Fig. 1. We assume that a solution containing species S_i ($1 \leq i \leq n$) is constantly injected into Inlet i with concentration $C_{S_{i_0}}$, average velocity v_{eff_i} , and volumetric flow rate Q_i . According to the well-known analogy between Hagen-Poiseuille's law and Ohm's law, the pressure drop, the flow rate, and the flow resistance in hydraulic circuits are analogous to the voltage drop, the electric current, and the electric resistance in electric circuits, respectively. On the one hand, this analogy enables a sound engineering estimate of steady-state pressure drops, flow rates, and hydraulic resistance of 1D long and straight microchannels, and is still effective even for channels with non-circular cross-sections that are neither perfectly straight nor infinite in extent. On the other hand, this analogy enables the application of electric circuit theory to microchannel network analysis [30]. Based on the *Kirchhoff's Current Law*, the volumetric flow rate in the n th combining

channel $Q^{\text{CH}n}$ is the summation of coming flow rates, such that

$$\begin{cases} Q^{\text{CH}1} = Q_1, \\ Q^{\text{CH}2} = Q^{\text{CH}1} + Q_2 = \sum_{i=1}^2 Q_i, \\ \dots, \\ Q^{\text{CH}n} = Q^{\text{CH}(n-1)} + Q_n = \sum_{i=1}^n Q_i. \end{cases} \quad (2)$$

Therefore, the mixed concentrations of species S_1 and S_2 in the second combining channel are [30]

$$\begin{cases} C_{S_1}^{\text{CH}2} = \frac{Q_1}{Q_1+Q_2} C_{S_{10}}, \\ C_{S_2}^{\text{CH}2} = \frac{Q_2}{Q_1+Q_2} C_{S_{20}}. \end{cases} \quad (3)$$

Then, when $n \geq 3$, the mixed concentrations of species S_1, S_2, \dots, S_n in the n th combining channel become

$$\begin{cases} C_{S_1}^{\text{CH}n} = \frac{Q^{\text{CH}(n-1)}}{Q^{\text{CH}(n-1)}+Q_n} C_{S_1}^{\text{CH}(n-1)} = \frac{\sum_{i=1}^{n-1} Q_i}{\sum_{i=1}^n Q_i} C_{S_1}^{\text{CH}(n-1)}, \\ C_{S_2}^{\text{CH}n} = \frac{Q^{\text{CH}(n-1)}}{Q^{\text{CH}(n-1)}+Q_n} C_{S_2}^{\text{CH}(n-1)} = \frac{\sum_{i=1}^{n-1} Q_i}{\sum_{i=1}^n Q_i} C_{S_2}^{\text{CH}(n-1)}, \\ \dots, \\ C_{S_n}^{\text{CH}n} = \frac{Q_n}{Q^{\text{CH}(n-1)}+Q_n} C_{S_{n0}} = \frac{Q_n}{\sum_{i=1}^n Q_i} C_{S_{n0}}. \end{cases} \quad (4)$$

Lemma 1. For the fluid mixing from n inlets to one combining channel, the mixed concentration of species S_i ($1 \leq i \leq n$) can be derived as

$$C_{S_i}^{\text{CH}n} = \frac{Q_i}{\sum_{i=1}^n Q_i} C_{S_{i0}}, \quad (5)$$

where Q_i and $C_{S_{i0}}$ are the volumetric flow rate and the species concentration injected into Inlet i . If all the species are injected with volumetric flow rate Q (i.e., $Q_1 = \dots = Q_n = Q$), species S_i will be diluted to $1/n$ of its injected concentration in the n th combining channel, that is

$$C_{S_i}^{\text{CH}n} = C_{S_{i0}}/n. \quad (6)$$

Proof. The last line of (4) can be reduced to (5) using (3) and other equations in (4). \square

Remark 1. From (6), we can conclude that a higher volume of injected fluids can lead to a decrease of the output concentration of each species.

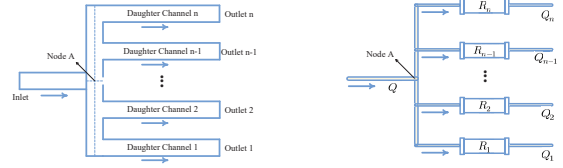
2) *Velocity Change:* Injecting fluids into a combining channel influences not only the species concentration but also the flow velocity.

Lemma 2. For the fluid mixing from n inlets to one combining channel, the flow rate in the n th combining channel can be expressed in terms of average velocity and channel geometry as

$$\begin{aligned} & w^{\text{CH}n} h^{\text{CH}n} v_{\text{eff}}^{\text{CH}n} \\ &= w^{\text{CH}(n-1)} h^{\text{CH}(n-1)} v_{\text{eff}}^{\text{CH}(n-1)} + w_n h_n v_{\text{eff}n}, \end{aligned} \quad (7)$$

where $v_{\text{eff}n}$, w_n , and h_n are the average velocity, the width, and the height of Inlet n , and $v_{\text{eff}}^{\text{CH}n}$, $w^{\text{CH}n}$, and $h^{\text{CH}n}$ are the average velocity, the width, and the height of the n th combining channel, respectively. If all inlets and combining channels share the same geometry and the same average velocity v_{eff} , the average velocity in the n th combining channel becomes

$$v_{\text{eff}}^{\text{CH}n} = n v_{\text{eff}}. \quad (8)$$



(a) A microfluidic device (b) Hydraulic circuit analog
Fig. 2. A microfluidic device for fluid separation analysis.

Proof. Based on the Kirchhoff's Current Law and (1), we can obtain (7). \square

Remark 2. It is revealed in (8) that a higher volume of injected fluids can lead to an increase of the average velocity.

B. Fluid Separation at Bifurcation Connections

In a microfluidic circuit, a single flow can be separated into different flow streams at a bifurcation connection, and we name this behavior as fluid separation for simplicity. Let us consider a microfluidic device with one inlet and n outlets as shown in Fig. 2(a), where a single flow is separated into n streams travelling over n daughter channels. Assuming that the solution containing species S_1 is injected with concentration $C_{S_{10}}$ and average velocity v_{eff} , the concentration at each outlet is the same as $C_{S_{10}}$, because species S_1 is not diluted by other species. However, the average velocity in each outlet varies for different geometry of its daughter channel. To derive the outlet velocities, we establish the hydraulic circuit model in Fig. 2(b). Analogous to current division in electric circuits, the relationship between the volumetric flow rate Q_i ($1 \leq i \leq n$) and the supplied volumetric flow rate Q can be described by [30, eq. (18)]

$$Q_i = R_{eq} Q / R_i, \quad (9)$$

where R_i is the hydraulic resistance of the i th daughter channel and R_{eq} is the equivalent resistance of all daughter channels. Let us denote L_{D_i} as the length from the crosspoint Node A in Fig. 2(b) to outlet i , and w_i and h_i as the geometry width and height of the i th daughter channel, R_i [30, eq. (10)] and R_{eq} [30, eq. (13)] can be calculated as

$$R_i = \frac{12\eta L_{D_i}}{w_i h_i^3 \left[1 - \sum_{i=1,3,5,\dots} \frac{192 h_i}{w_i \pi^5 i^5} \tan h_i \left(\frac{i\pi w_i}{2h_i} \right) \right]}, \quad (10)$$

$$\text{and } R_{eq} = 1/(1/R_1 + 1/R_2 + \dots + 1/R_n). \quad (11)$$

Lemma 3. For the fluid separation from one inlet to n outlets, the average velocity $v_{\text{eff}i}$ in the i th outlet can be derived as

$$v_{\text{eff}i} = \frac{R_{eq}}{R_i} \frac{wh}{w_i h_i} v_{\text{eff}}, \quad (12)$$

where w and h are the width and the height of the injection channel, w_i and h_i are the width and the height of the i th daughter channel, R_i and R_{eq} are given in (10) and (11), respectively. If all daughter channels share the same geometry (i.e., $w_1 h_1 = \dots = w_n h_n = wh$ and $L_{D_1} = \dots = L_{D_n}$), eq. (12) can be reduced to

$$v_{\text{eff}i} = v_{\text{eff}}/n. \quad (13)$$

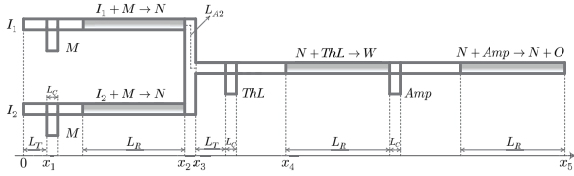


Fig. 3. The chemical reactions-based microfluidic AND logic gate. To distinguish convection-diffusion channels and convection-diffusion-reaction channels, the latter are filled with grey-gradient color.

Proof. Substituting (1) into (9), we can obtain (12). When all daughter channels share the same geometry, $R_i = nR_{eq}$ and thus (12) can be reduced to (13). \square

Remark 3. It is indicated from (13) that fluid separation results in a reduction of average velocity by n times.

III. AND LOGIC GATE DESIGN AND ANALYSIS

In this section, we present the design of the AND logic gate to demonstrate the logic computation ability of microfluidic circuits. The chemical reactions used in the AND gate can be categorized into two forms: 1) $S_i + S_j \rightarrow S_k$, and 2) $S_i + Amp \rightarrow S_i + O$. For a reaction with the form of $S_i + S_j \rightarrow S_k$, species S_i is consumed by species S_j and the residual species S_i will be the part that is above the concentration of species S_j . Hence, the concentration of species S_j can be regarded as a threshold for species S_i and we name this reaction as a thresholding reaction. For a reaction with the form of $S_i + Amp \rightarrow S_i + O$, species O is only produced in the presence of S_i and the concentration of species O equals the injected concentration of species Amp . This property allows us to amplify the amount of species O to any desired level by adjusting the concentration of species Amp , and thus we name this reaction as an amplifying reaction [31].

We present our proposed **AND gate design** in Fig. 3. As shown in Fig. 3, the proposed AND gate consists of the input species I_1 and I_2 , and the output species O . Throughout this paper, we use non-zero concentration to represent HIGH state (bit-1), and zero concentration to represent LOW state (bit-0). Moreover, we assume that the flows carrying chemical species are laminar, which is a valid assumption in microfluidic settings [3]. The two input species I_1 and I_2 are first converted to an intermediate species N , so the state of species N will be HIGH if either I_1 or I_2 is HIGH. Then, species N flows into the reaction channel with reaction $N + ThL \rightarrow W$ and undergoes a depletion by species ThL . By injecting a certain amount of species ThL , the remaining concentration of species N can be larger than zero only when both input species I_1 and I_2 are HIGH. Finally, the remaining species N catalyzes the conversion of species Amp to output species O via reaction $N + Amp \rightarrow N + O$, and the concentration of species O can be adjusted to a desired level based on the injected concentration of species Amp .

To derive the output concentration of our designed AND gate, we first need to study the molecule concentration distribution in a *single* channel. For a 3D straight microfluidic channel, if molecule transport is in the dispersion regime, molecules will be uniformly distributed across the cross-section. Thus, the molecule concentration can be described

by a simplified 1D convection-diffusion-reaction equation as [3, eq. (29)]

$$\frac{\partial C_{S_i}(x, t)}{\partial t} = D_{\text{eff}} \frac{\partial^2 C_{S_i}(x, t)}{\partial x^2} - v_{\text{eff}} \frac{\partial C_{S_i}(x, t)}{\partial x} + qf[k, C_{S_i}(x, t)], \quad (14)$$

where $C_{S_i}(x, t)$ is the spatial-temporal concentration of species S_i ; D_{eff} is the *Taylor-Aris* effective diffusion coefficient; v_{eff} is the average velocity; $q = 1$ and $q = -1$ hold if species S_i is the product and the reactant of any reaction, respectively; k is the rate constant and $f[\cdot]$ is the reaction term that in general can account for the presence of multiple reactions. For a microfluidic channel with rectangular-shaped cross-section¹, D_{eff} can be calculated as [32, eq. (3)]

$$D_{\text{eff}} = \left[1 + \frac{8.5v_{\text{eff}}^2 h^2 w^2}{210D^2(h^2 + 2.4hw + w^2)} \right] D, \quad (15)$$

where h is the cross-section height, w is the cross-section width, and D is the molecular diffusion coefficient.

When $k = 0$, eq. (14) reduces to a convection-diffusion equation. In the following, we first derive the impulse response of a convection-diffusion channel in Sec. III-A. Based on the impulse response, we then study the molecule concentration of a reaction channel either with a thresholding reaction (Sec. III-B), or an amplifying reaction (Sec. III-C). Furthermore, relying on the analysis in Sec. II, we define and model four elementary blocks (Sec. III-D) in order to simplify the theoretical characterizations of the AND gate in Sec. III-E and the more complicated microfluidic circuits proposed in Sec. IV.

A. Convection-Diffusion Channel

Without chemical reactions, the concentration distribution of species S_i can be expressed using a convection-diffusion equation as [3, eq. (29)]

$$\frac{\partial C_{S_i}(x, t)}{\partial t} = D_{\text{eff}} \frac{\partial^2 C_{S_i}(x, t)}{\partial x^2} - v_{\text{eff}} \frac{\partial C_{S_i}(x, t)}{\partial x}. \quad (16)$$

Although (16) has been solved in [27], the complex expression of the solution does not allow the cascaded channels to be mathematically solvable in closed-form. This shortcoming motivates us to derive the impulse response of a microfluidic channel so that the output of a microfluidic circuit can be written as the convolution of an input and a cascade of the impulse response of each channel. We solve the impulse response in the following theorem.

Theorem 1. The impulse response of a straight convection-diffusion channel is derived as

$$H(x, t) = \frac{1}{2\pi} \int_0^\infty [e^{-j\omega t} \widetilde{C}_{S_i}(x, \omega) + e^{j\omega t} \widetilde{C}_{S_i}(x, \omega)] d\omega, \quad (17)$$

where

$$\begin{aligned} & \widetilde{C}_{S_i}(x, \omega) \\ &= \exp \left[(v_{\text{eff}} x / 2D_{\text{eff}}) - \sqrt{x^2 (v_{\text{eff}}^2 + 4j\omega D_{\text{eff}}) / 4D_{\text{eff}}^2} \right] \end{aligned} \quad (18)$$

¹The rectangular-shaped cross-section is a common geometry considered in MC literature [32]–[34]. The methodology presented in this paper can be also applied to other cross-section shapes.

and $\widetilde{C_{S_i}}(x, \omega)$ is the complex conjugate of $\widetilde{C_{S_i}}(x, \omega)$.

Proof. Please refer to the Appendix A. \square

From **Theorem 1**, the concentration of species S_i can be expressed as

$$C_{S_i}(x, t) = C_{S_{i_0}}(t) * H(x, t), \quad (19)$$

where $C_{S_{i_0}}(t)$ is the input concentration of species S_i at channel inlet and “*” denotes the convolution operator.

B. Reaction Channel with a Thresholding Reaction

When a microfluidic channel contains a thresholding reaction $S_i + S_j \rightarrow S_k$, according to (14) and [35, eq. (9.13)], the spatial-temporal concentration distributions of reactant and product are

$$\begin{aligned} \frac{\partial C_{S_i}(x, t)}{\partial t} &= D_{\text{eff}} \frac{\partial^2 C_{S_i}(x, t)}{\partial x^2} \\ &\quad - v_{\text{eff}} \frac{\partial C_{S_i}(x, t)}{\partial x} - k C_{S_i}(x, t) C_{S_j}(x, t), \end{aligned} \quad (20)$$

$$\begin{aligned} \frac{\partial C_{S_k}(x, t)}{\partial t} &= D_{\text{eff}} \frac{\partial^2 C_{S_k}(x, t)}{\partial x^2} \\ &\quad - v_{\text{eff}} \frac{\partial C_{S_k}(x, t)}{\partial x} + k C_{S_i}(x, t) C_{S_j}(x, t). \end{aligned} \quad (21)$$

Compared with the convection-diffusion equation in (16), the newly introduced reaction term is fully coupled with convection and diffusion process, which complicates the resolution of (20) and (21). A strategy to tackle this coupling is to apply the “operator splitting” method. It first divides an original differential equation into several sub-equations, which are solved separately to give their individual solutions. Then, the solutions for sub-equations are combined to form a solution for the original equation [36]. The derived impulse response of a convection-diffusion channel in **Theorem 1** motivates us to separate a convection-diffusion-reaction equation into a reaction term and a convection-diffusion term. This separation can be achieved via 1) assuming the reactants are added into a virtual reactor, and the unconsumed reactants and generated product flow into a convection-diffusion channel as soon as the reaction stops; and 2) treating the solution of the reaction term as the initial input for the convection-diffusion part.

With species S_i and S_j continuously flowing into a channel, we regard that S_i and S_j are continuously added into a virtual reactor, where the continuous reactant supply is a superposition of reactant addition with constants at different times. To solve the reaction part, we consider the following two scenarios:

- **Scenario 1:** species S_i and S_j are only added at $t = 0$ with concentration $C_{S_{i_0}}$ and $C_{S_{j_0}}$;
- **Scenario 2:** species S_i and S_j are added continuously with concentration $C_{S_{i_0}}(t)$ and $C_{S_{j_0}}(t)$.

We first derive the concentration changes of reactants and product for **Scenario 1**, which will then be applied to **Scenario 2** to derive the solutions of the separated reaction term.

1) **Scenario 1:** Let $c(t)$ denote the consumed concentration of reactant S_i or S_j during the reaction. Note that $c(t)$ can also represent the concentration of product species S_k due to a one-to-one stoichiometric relation between reactants and product.

The remaining concentrations of species S_i and S_j can be expressed as

$$C_{S_i}(t) = C_{S_{i_0}} - c(t), \quad (22a)$$

$$C_{S_j}(t) = C_{S_{j_0}} - c(t). \quad (22b)$$

Then, the reaction equation can be expressed as [35, eq. (9.13)]

$$d[C_{S_{i_0}} - c(t)]/dt = -k[C_{S_{i_0}} - c(t)][C_{S_{j_0}} - c(t)]. \quad (23)$$

After rearrangement, eq. (23) becomes

$$\frac{dc(t)}{[C_{S_{i_0}} - c(t)][C_{S_{j_0}} - c(t)]} = k dt. \quad (24)$$

By taking the integral of the two sides of (24), we yield

$$c(t) = \begin{cases} \frac{C_{S_{i_0}} C_{S_{j_0}} \exp[(C_{S_{j_0}} - C_{S_{i_0}})kt] - C_{S_{i_0}} C_{S_{j_0}}}{C_{S_{j_0}} \exp[(C_{S_{j_0}} - C_{S_{i_0}})kt] - C_{S_{i_0}} C_{S_{j_0}}}, & C_{S_{i_0}} \leq C_{S_{j_0}}, \\ \frac{C_{S_{i_0}} C_{S_{j_0}} \exp[(C_{S_{i_0}} - C_{S_{j_0}})kt] - C_{S_{i_0}} C_{S_{j_0}}}{C_{S_{i_0}} \exp[(C_{S_{i_0}} - C_{S_{j_0}})kt] - C_{S_{i_0}} C_{S_{j_0}}}, & C_{S_{i_0}} \geq C_{S_{j_0}}. \end{cases} \quad (25)$$

Remark 4. It can be observed from (25) that $c(t)$ is proportional to the rate constant k . The higher the rate constant is, the faster a reactant is consumed and decreased to zero.

Lemma 4. For reaction $S_i + S_j \rightarrow S_k$, when reaction rate $k \rightarrow \infty$, the consumed concentration $c(t)$ of reactant can be derived as

$$\lim_{k \rightarrow \infty} c(t) = \varphi(C_{S_{i_0}}, C_{S_{j_0}}), \quad (26)$$

where $C_{S_{i_0}}$ and $C_{S_{j_0}}$ are the initial concentrations of species S_i and S_j , and $\varphi(\cdot, \cdot)$ is defined as

$$\varphi(x, y) = \min\{x, y\}. \quad (27)$$

Proof. With $k \rightarrow \infty$, eq. (25) can be easily reduced to (26). \square

2) **Scenario 2:** Now, we consider the continuous injection of species S_i and S_j with concentrations $C_{S_{i_0}}(t)$ and $C_{S_{j_0}}(t)$. **Scenario 2** can be regarded as a superposition of **Scenario 1** in time domain. To apply the analysis of **Scenario 1**, we first discretize the reaction process into many time intervals with step Δt . Thus, the added concentration of species S_i can be denoted as $C_{S_{i_0},a}^n = C_{S_{i_0}}(n\Delta t)$ ($n \geq 0$), where the subscript a refers to addition.² We also denote $C_{S_{i_0}}^n$ and $C_{S_{i_0},r}^n$ as the initial and the remaining concentrations of S_i at $t = n\Delta t$, respectively. The same notations are also applied to species S_j .

We propose **Algorithm 1** to numerically calculate the remaining concentrations of S_i and S_j for reaction $S_i + S_j \rightarrow S_k$. **Algorithm 1** describes that for any time interval $[n\Delta t, (n+1)\Delta t]$, the consumed concentration can be calculated according to (25), but with different initial concentrations $C_{S_{i_0}}^n$. The difference in the initial concentration is due to the fact that the initial concentration of any time interval is influenced not only by the newly added concentration, but also by the incompletely consumed concentration that added in previous intervals. For instance, the initial concentration $C_{S_{i_0}}^1$ for the time interval $[\Delta t, 2\Delta t]$ is the sum of the newly

²Throughout this paper, the superscript for concentration C does not represent a mathematical operation.

Algorithm 1: The Calculation of Remaining Concentrations of Species S_i and S_j

Input: The input concentrations $C_{S_{i_0}}(t)$ and $C_{S_{j_0}}(t)$.
The calculation time interval $[0, T]$. The time step Δt .

- 1 Initialization of $C_{S_{i_0}}^0 = C_{S_{i_0},a}^0$ and $C_{S_{j_0}}^0 = C_{S_{j_0},a}^0$.
 - 2 **for** $n \leftarrow 1, \lfloor T/\Delta t \rfloor$ **do**
 - 3 Calculate the consumed concentration c^{n-1} during $[(n-1)\Delta t, n\Delta t]$ according to (25) by interchanging $C_{S_{i_0}} \rightarrow C_{S_{i_0}}^{n-1}$ and $C_{S_{j_0}} \rightarrow C_{S_{j_0}}^{n-1}$.
 - 4 Update the remaining concentration $C_{S_{i_0},r}^n = C_{S_{i_0}}^{n-1} - c^{n-1}$ and $C_{S_{j_0},r}^n = C_{S_{j_0}}^{n-1} - c^{n-1}$.
 - 5 Update the initial concentration $C_{S_{i_0}}^n = C_{S_{i_0},r}^n + C_{S_{i_0},a}^n$ and $C_{S_{j_0}}^n = C_{S_{j_0},r}^n + C_{S_{j_0},a}^n$ for $[n\Delta t, (n+1)\Delta t]$.
 - 6 **end**
-

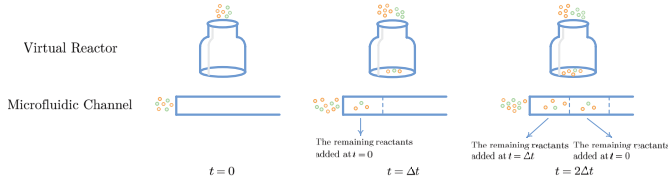


Fig. 4. Illustration of reaction $S_i + S_j \rightarrow S_k$ in a bottle-shaped virtual reactor and a microfluidic channel. The two reactants are marked with different colors.

added concentration $C_{S_{i_0},a}^1$ and the remaining concentration $C_{S_{i_0},r}^1$ that added at $t = 0$.

The value of rate constant k influences the approximation accuracy. The smaller the k is, the larger volume of reactants remain. The unconsumed reactants accumulate in reactor and would participate into the reaction in the following time interval, which introduces correlation between different time intervals. By contrast, this correlation does not exist in practical scenario. As shown in Fig. 4, for time interval $[\Delta t, 2\Delta t]$, the flowing fluid carries remaining reactants added at $t = 0$ and $t = \Delta t$ forward, preventing them from interacting with each other. Therefore, in the virtual reactor, we should make rate constant approach infinity to ensure that reaction is always complete inside any time interval, thus eliminating the correlation³. With $\Delta t \rightarrow 0$, the remaining concentrations of S_i and S_j calculated in **Algorithm 1** reduce to

$$C_{S_{i_0},r}(t) = C_{S_{i_0}}(t) - \varphi[C_{S_{i_0}}(t), C_{S_{j_0}}(t)], \quad (28a)$$

$$C_{S_{j_0},r}(t) = C_{S_{j_0}}(t) - \varphi[C_{S_{i_0}}(t), C_{S_{j_0}}(t)], \quad (28b)$$

where $\varphi(\cdot, \cdot)$ is given in (27).

We derive the output concentrations of species S_i , S_j and S_k in the following lemma.

Lemma 5. For a straight reaction channel with thresholding reaction $S_i + S_j \rightarrow S_k$, the output concentrations of species

³In order to eliminate the correlation between different time intervals, the assumption $k \rightarrow \infty$ is only made in **Algorithm 1**. In practice, k cannot be infinity and k should be selected to ensure that a reaction is complete for a given microfluidic channel. Otherwise, there will be a disagreement between our theoretical analysis and the simulation results under low rate constant region.

S_i , S_j , and S_k can be derived as

$$C_{S_i}(x, t) = C_{S_{i_0},r}(t) * H(x, t), \quad (29a)$$

$$C_{S_j}(x, t) = C_{S_{j_0},r}(t) * H(x, t), \quad (29b)$$

$$C_{S_k}(x, t) = \varphi[C_{S_{i_0}}(t), C_{S_{j_0}}(t)] * H(x, t), \quad (29c)$$

where $C_{S_{i_0},r}(t)$, $C_{S_{j_0},r}(t)$, $H(x, t)$, and $\varphi(\cdot, \cdot)$ are given in (28a), (28b), (17), and (27), respectively.

Proof. Recall that we separate a convection-diffusion-reaction equation into a reaction part and a convection-diffusion part, we consider the remaining concentrations of S_i in (28a) and S_j in (28b) as inputs to a straight convection-diffusion channel. According to (19), we can obtain (29a) and (29b). The derivation of (29c) can see Appendix B. \square

C. Reaction Channel with an Amplifying Reaction

Lemma 6. For a straight reaction channel with amplifying reaction $S_i + Amp \rightarrow S_i + O$, the output concentration of species O can be derived as

$$C_O(x, t) = [C_{Amp_0}(t) \cdot \mathbb{1}_{\{C_{S_{i_0}}(t) > 0\}}] * H(x, t), \quad (30)$$

where $C_{Amp_0}(t) = C_{Amp_0}u(t)$ and $C_{S_{i_0}}(t)$ are the injected concentrations of species Amp and S_i , $u(t)$ is the Heaviside step function, $\mathbb{1}_{\{\cdot\}}$ is the indicator function that represents the value 1 if the statement is true, and zero otherwise.

Proof. To analyze a straight microfluidic channel with amplifying reaction $S_i + Amp \rightarrow S_i + O$, we also separate it into a reaction term and a convection-diffusion term. For the reaction term, as species O is only produced in the presence of S_i and the concentration of species O equals the injected concentration of species Amp [31], the reaction solution can be expressed as $C_{Amp_0}(t) \cdot \mathbb{1}_{\{C_{S_{i_0}}(t) > 0\}}$. Taking the reaction solution as the initial input for a convection-diffusion channel, we derive the concentration of product O in (30). \square

D. Elementary Blocks

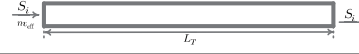
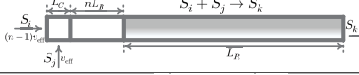
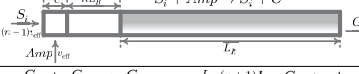
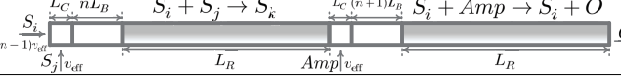
Relying on the analyses of fluid mixing in **Lemma 1 and 2**, convection-diffusion channel in **Theorem 1**, and convection-diffusion-reaction channel in **Lemma 5 and 6**, we focus on the analysis of four elementary blocks of our designed AND gate (Fig. 3) in Table I. Meanwhile, to simplify the output expression of a microfluidic circuit, we also define five typical operators for the four elementary blocks. As shown in Table I, the operator $\mathcal{T}[\cdot]$ represents the output of a convection-diffusion channel with length L_T , and can be expressed as

$$\mathcal{T}[C_{S_{i_0}}(t), n] \triangleq C_{S_{i_0}}(t) * H_n(L_T, t), \quad (31)$$

where the subscript n of H_n indicates that the average velocity in the channel is nv_{eff} .

For the block with thresholding reaction $S_i + S_j \rightarrow S_k$, solutions containing species S_i and S_j are injected to a channel with length L_C from two inlets. The initial concentrations of species S_i and S_j are $C_{S_{i_0}}(t)$ and $C_{S_{j_0}}(t)$, and the injection speeds of species S_i and S_j are $(n-1)v_{\text{eff}}$ and v_{eff} . The combining of two solutions will result in a concentration dilution, and the diluted concentrations of S_i and S_j are $(n-1)C_{S_{i_0}}(t)/n$ and $C_{S_{j_0}}(t)/n$ following (5) in **Lemma 1**, respectively. Meanwhile, the average velocity will increase

TABLE I
FOUR ELEMENTARY BLOCKS.

Operator	Elementary Block	Operator Output
$\mathcal{T}[C_{S_{i_0}}(t), n]$ Eq. (31)		$C_{S_k}(t)$: The output of a convection-diffusion channel with length L_T .
$\mathcal{G}[C_{S_{i_0}}(t), C_{S_{j_0}}(t), n]$ Eq. (33)		$C_{S_k}(t)$: The concentration of product S_k with $S_i + S_j \rightarrow S_k$.
$\mathcal{R}[C_{S_{i_0}}(t), C_{S_{j_0}}(t), n]$ Eq. (34)		$C_{S_i}(t)$: The remaining concentration of S_i with $S_i + S_j \rightarrow S_k$.
$\mathcal{A}[C_{S_{i_0}}(t), C_{Amp_0}(t), n]$ Eq. (35)		$C_O(t)$: The concentration of product O with $S_i + Amp \rightarrow S_i + O$.
$\mathcal{F}[C_{S_{i_0}}(t), C_{S_{j_0}}(t), C_{Amp_0}(t), n]$ Eq. (36)		$C_O(t)$: The concentration of product O with $S_i + S_j \rightarrow S_k$ and $S_i + Amp \rightarrow S_i + O$.

to nv_{eff} following (7) in **Lemma 2**. Then, species will flow to a buffer channel before the convection-diffusion-reaction channel filled with grey-gradient color.⁴ The buffer channel allows reactants to be well mixed before a reaction, and the reactant mixing along the radial direction only relies on diffusion. The minimum buffer length L_B can be estimated as

$$L_B = \frac{w^2 + h^2}{D} v_{\text{eff}}. \quad (32)$$

The term $\frac{w^2 + h^2}{D}$ quantifies the time required for molecules to be transported over distance $\sqrt{w^2 + h^2}$ along the radial direction to achieve a fully diffusional mixing, and (32) represents how far molecules have traveled along the axial direction by convection. We define operator $\mathcal{G}[\cdot]$ to describe the concentration of product S_k , and according to (29c), operator $\mathcal{G}[\cdot]$ can be expressed as

$$\begin{aligned} & \mathcal{G}[C_{S_{i_0}}(t), C_{S_{j_0}}(t), n] \\ & \triangleq \varphi[(n-1)C_{S_{i_0}}(t)/n, C_{S_{j_0}}(t)/n] \\ & * H_n(nL_B + L_C, t) * H_n(L_R, t). \end{aligned} \quad (33)$$

For the same reaction, we define operator $\mathcal{R}[\cdot]$ to characterize the residual concentration of S_i . According to (29a), operator $\mathcal{R}[\cdot]$ can be expressed as

$$\begin{aligned} & \mathcal{R}[C_{S_{i_0}}(t), C_{S_{j_0}}(t), n] \\ & \triangleq [(n-1)C_{S_{i_0}}(t)/n - \varphi[(n-1)C_{S_{i_0}}(t)/n, C_{S_{j_0}}(t)/n]] \\ & * H_n(nL_B + L_C, t) * H_n(L_R, t). \end{aligned} \quad (34)$$

For the amplifying reaction $S_i + Amp \rightarrow S_i + O$, operator $\mathcal{A}[\cdot]$ describes the concentration of product O , and can be expressed using **Lemma 6** as

$$\begin{aligned} & \mathcal{A}[C_{S_{i_0}}(t), C_{Amp_0}(t), n] \\ & \triangleq [C_{Amp_0}(t)/n * H_n(nL_B + L_C, t)] \\ & \cdot \mathbb{1}_{\{[(n-1)C_{S_{i_0}}(t)/n] * H_n(nL_B + L_C, t) > 0\}} * H_n(L_R, t). \end{aligned} \quad (35)$$

As seen in the AND gate design in Fig. 3, a threshold reaction is cascaded with an amplifying reaction; thus, we define operator $\mathcal{F}[\cdot]$ as a combination of operators $\mathcal{R}[\cdot]$ and

⁴In practice, by cooling the buffer channel while heating the corresponding reaction channel, it would allow us to keep the buffer channel thermally isolated from the reaction channel, which ensures that pre-mixed reactants do not react until they reach the reaction channel [37].

$\mathcal{A}[\cdot]$, which represents the concentration of product O with $S_i + S_j \rightarrow S_k$ and $S_i + Amp \rightarrow S_i + O$ as

$$\begin{aligned} & \mathcal{F}[C_{S_{i_0}}(t), C_{S_{j_0}}(t), C_{Amp_0}(t), n] \\ & \triangleq \mathcal{A}[\mathcal{R}[C_{S_{i_0}}(t), C_{S_{j_0}}(t), n], C_{Amp_0}(t), n + 1]. \end{aligned} \quad (36)$$

E. AND Logic Gate Analysis

We denote the initial concentrations of input species I_1 and I_2 as $C_{I_{1_0}}(t)$ and $C_{I_{2_0}}(t)$. Remind that we use non-zero concentration to represent HIGH state (bit-1), and zero concentration to represent LOW state (bit-0). Therefore, at any time t , $C_{I_{1_0}}(t)$ and $C_{I_{2_0}}(t)$ are either greater than or equal to 0. Species M , ThL , and Amp are injected continuously; thus, their initial concentrations follow $C_{M_0}(t) = C_{M_0}u(t)$, $C_{ThL_0}(t) = C_{ThL_0}u(t)$, and $C_{Amp_0}(t) = C_{Amp_0}u(t)$. For simplicity, all reactants are injected using the same average velocity v_{eff} .

Theorem 2. *The concentration of product species O in our designed AND gate in Fig. 3 can be derived as*

$$\begin{aligned} & C_O(x_5, t) \\ & = \mathcal{F}\{\mathcal{T}[C_N(x_3, t), 4], \mathcal{T}[C_{ThL_0}(t), 1], \mathcal{T}[C_{Amp_0}(t), 1], 5\}, \end{aligned} \quad (37)$$

where

$$\begin{aligned} & C_N(x_3, t) \\ & = \frac{1}{2} \{ \mathcal{G}[\mathcal{T}[C_{I_{1_0}}(t), 1], \mathcal{T}[C_{M_0}(t), 1], 2] \\ & + \mathcal{G}[\mathcal{T}[C_{I_{2_0}}(t), 1], \mathcal{T}[C_{M_0}(t), 1], 2] \} * H_2(L_{A2}, t). \end{aligned} \quad (38)$$

In (37) and (38), operators $\mathcal{T}[\cdot]$, $\mathcal{G}[\cdot]$, $\mathcal{F}[\cdot]$ are defined in Table I, L_{A2} is the travelling distance of the laminar located at the centre channel from x_2 to x_3 in Fig. 3.

Proof. To facilitate the understanding of the derivation, we illustrate the flow velocity changes and the mathematical descriptions of some elementary blocks in Fig. 5. At position $x = x_1$, the concentrations of species I_1 and I_2 can be expressed as $\mathcal{T}[C_{I_{1_0}}(t), 1]$ and $\mathcal{T}[C_{I_{2_0}}(t), 1]$, respectively. Then, species I_1 (or I_2) and M flow into the second elementary block defined in Table I, and the output product species N can be described using operator $\mathcal{G}[\cdot]$, that is: $\mathcal{G}[\mathcal{T}[C_{I_{1_0}/I_{2_0}}(t), 1], \mathcal{T}[C_{M_0}(t), 1], 2]$. The species N separately generated by inputs I_1 and I_2 merge with each other at position $x = x_3$. The concentration of species N at $x = x_3$ can be derived as (38), where the coefficient $1/2$ explains

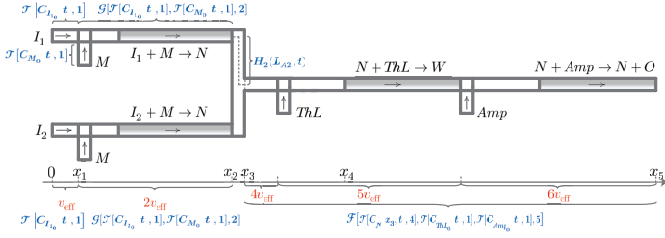


Fig. 5. An illustration of the theoretical characterization of our proposed AND gate design in Fig. 3 using the four elementary blocks and five operators in Table I. The average velocity changes are marked using red font.

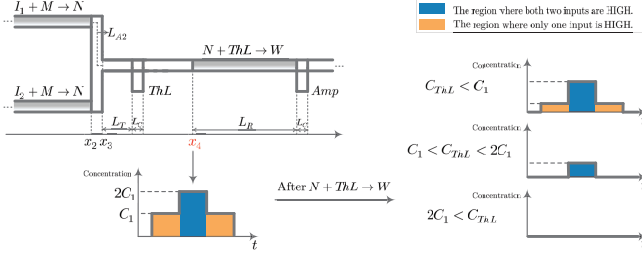


Fig. 6. The concentration of species N before and after the reaction $N + ThL \rightarrow W$ in the designed AND gate.

the dilution of species N generated in the upper branch by the flow in the lower branch, or vice versa. Finally, species N travels over a convection-diffusion channel and enters the elementary block $\mathcal{F}[\cdot]$ consisting of reactions $N + ThL \rightarrow W$ and $N + Amp \rightarrow N + O$ to produce the gate output O . According to the definition of $\mathcal{F}[\cdot]$ in (36), the concentration of species O at location $x = x_5$ can be derived as (37). \square

For the thresholding reaction $N + ThL \rightarrow W$ in Fig. 5, C_{ThL_0} directly determines the gate function. We derive the constraint for C_{ThL_0} in the following lemma.

Lemma 7. *To ensure that the designed microfluidic circuit exhibits AND logic behavior, the concentration of species ThL needs to satisfy*

$$C_{Con} < C_{ThL_0} < 2C_{Con}, \quad (39)$$

where

$$C_{Con} = \frac{\lim_{t \rightarrow \infty} 2\mathcal{G}\{\mathcal{T}[C_0 u(t), 1], \mathcal{T}[C_{M_0} u(t), 1], 2\} * q(t)}{\lim_{t \rightarrow \infty} \mathcal{T}[u(t), 1] * H_5(5L_B + L_C, t)}. \quad (40)$$

In (40), C_0 is the HIGH concentration of input species I_1 and I_2 , C_{M_0} is the HIGH concentration of species M , $q(t) = H_2(L_{A2}, t) * H_4(L_T, t) * H_5(5L_B + L_C, t)$, $H(x, t)$ is the impulse response derived in (17), and $\mathcal{T}[\cdot]$ and $\mathcal{G}[\cdot]$ are defined in (31) and (33), respectively.

Proof. Let C_1 and C_{ThL} denote the steady-state concentrations of species N and ThL at location $x = x_4$, respectively. Fig. 6 plots the concentration of species N before and after reaction $N + ThL \rightarrow W$. When only one input is HIGH, the steady-state concentration C_1 can be expressed as

$$C_1 = \lim_{t \rightarrow \infty} \frac{4}{5} \cdot \frac{1}{2} \cdot \mathcal{G}\{\mathcal{T}[C_0 u(t), 1], \mathcal{T}[C_{M_0} u(t), 1], 2\} * q(t), \quad (41)$$

where the coefficient $4/5$ explains the dilution of species N by species ThL . When both inputs are HIGH, the steady-state

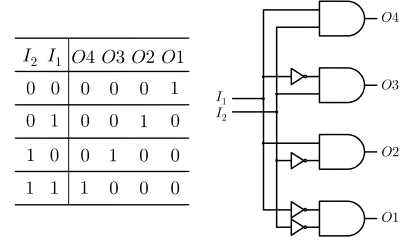


Fig. 7. The truth table and implementation of an electric 2:4 decoder.

concentration becomes $2C_1$. For species ThL , its steady-state concentration C_{ThL} at $x = x_4$ can be expressed as

$$C_{ThL} = \lim_{t \rightarrow \infty} \frac{1}{5} \mathcal{T}[C_{ThL_0} u(t), 1] * H_5(5L_B + L_C, t), \quad (42)$$

where the coefficient $1/5$ explains the dilution of species ThL by the flow coming from location x_3 . As shown in Fig. 6, the blue region represents that both two inputs are HIGH, and the yellow region represents that only one input is HIGH. The relationship between C_1 and C_{ThL} has three cases:

- $C_{ThL} < C_1$: After reaction, the remaining concentration of species N contains the region where one or both the inputs are HIGH.
- $C_1 < C_{ThL} < 2C_1$: After reaction, the remaining concentration of species N only contains the region where both two inputs are HIGH.
- $2C_1 < C_{ThL}$: After reaction, species N is completely depleted.

Therefore, to capture the region where both the inputs are HIGH, the concentration of species ThL needs to satisfy the condition $C_1 < C_{ThL} < 2C_1$. Combined with (41) and (42), we can obtain (39) and (40). \square

IV. MICROFLUIDIC QCSK TRANSMITTER AND RECEIVER

In this section, we present the microfluidic designs to show how logic computations can process molecular concentration so as to achieve QCSK modulation and demodulation. Meanwhile, we also theoretically characterize the output concentration distributions of the proposed QCSK transmitter and receiver. At the end, we discuss the synchronization of molecular species in microfluidic circuits.

A. QCSK Transmitter

1) *QCSK Transmitter Design:* QCSK modulation represents two digital inputs as four concentration levels of an output signal, which is analogous to the Amplitude Shift Keying (ASK) modulation in wireless communication [4]. A challenge of implementing a QCSK MC transmitter is how to control the output concentration via four different input combinations (i.e., “00”, “01”, “10”, and “11”). We solve this challenge by borrowing the mechanism of an electric 2:4 decoder. In electric circuits, a 2:4 decoder, which has 2 inputs and 4 outputs, selects exactly one of its outputs according to the input combination. Fig. 7 presents the truth table and an implementation of the electric 2:4 decoder, where four AND gates receive the HIGH or the LOW of inputs I_1 and I_2 .

Inspired by the electric 2:4 decoder, we propose a chemical reactions-based microfluidic 2:4 decoder (with a combiner) to realize QCSK modulation as shown in Fig. 8. The proposed

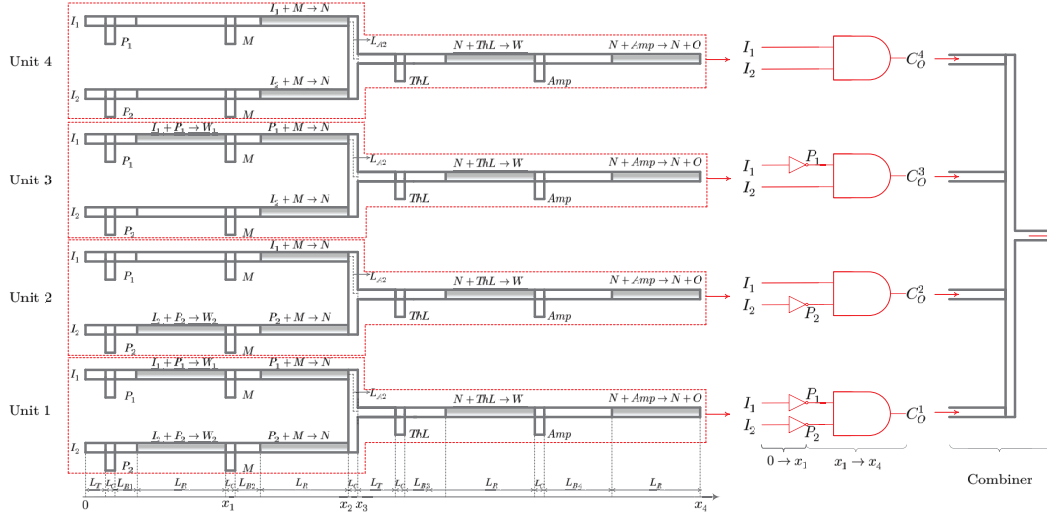


Fig. 8. The chemical reactions-based microfluidic 2:4 decoder.

microfluidic device is made up of four microfluidic units corresponding to four different concentration outputs. For ease of reference, these four units are named as Unit 4, Unit 3, Unit 2, and Unit 1 from top to bottom. Analogous to the electric 2:4 decoder in Fig. 7, the AND gate in each unit takes either I_1 and I_2 or their complementary species P_1 and P_2 as its inputs. Species P_1 and P_2 are supplied continuously with a HIGH state so that after reactions $I_1 + P_1 \rightarrow W_1$ and $I_2 + P_2 \rightarrow W_2$, the remaining concentrations of species P_1 and P_2 , i.e., $C_{P_1/P_2}(x_1, t)$, can represent the complementary states of species I_1 and I_2 , thus achieving the NOT gate. Unlike an electric 2:4 decoder that an identical voltage level is produced no matter which unit is selected, the proposed chemical 2:4 decoder will output different concentration levels. As each unit output $C_O^i(t)$ is influenced by $C_{Amp_0}^i$ through an amplifying reaction, the concentration variation of transmitted signals is represented via different concentrations of injected species Amp as $C_{Amp_0}^i(t) = C_{Amp_0}^i u(t)$ ($1 \leq i \leq 4$) for different units. Here, we set $C_{Amp_0}^4 > C_{Amp_0}^3 > C_{Amp_0}^2 > C_{Amp_0}^1$ to ensure $\max\{C_O^4(t)\} > \max\{C_O^3(t)\} > \max\{C_O^2(t)\} > \max\{C_O^1(t)\}$. The combiner acts as a transmitter-channel interface and merely combines the four outputs $C_O^i(t)$. We highlight that it does not have an impact on the QCSK modulation function. Thus, for simplicity we will not consider it in the following analysis, which also brings flexibility to test each unit of our proposed design.

2) *QCSK Transmitter Analysis*: The objective of the following analysis is to derive the transmitter output $C_O^i(t)$ of the design in Fig. 8. We first derive the inputs of an AND gate, i.e., the concentrations of I_1 , I_2 , P_1 , and P_2 at location $x = x_1$. When input species I_1 and I_2 directly flow into an AND gate, their concentrations can be expressed as

$$C_{I_1/I_2}(x_1, t) = [\mathcal{T}[C_{I_{1_0}/I_{2_0}}(t), 1] * H_2(L_C + L_{B1} + L_R, t)]/2, \quad (43)$$

where $C_{I_{1_0}/I_{2_0}}(t)$ is the concentration of input species I_1 or I_2 , operator $\mathcal{T}[\cdot]$ is defined in Table I, the coefficient $1/2$ explains the dilution of species I_1 by species P_1 (or I_2 by

P_2). When the complementary species P_1 and P_2 flow into an AND gate, their concentrations can be expressed as

$$C_{P_1/P_2}(x_1, t) = \mathcal{R}\{\mathcal{T}[C_{P_{1_0}/P_{2_0}}(t), 1], \mathcal{T}[C_{I_{1_0}/I_{2_0}}(t), 1], 2\}, \quad (44)$$

where $C_{P_{1_0}/P_{2_0}}(t)$ is the input concentration of species P_1 or P_2 , and operator $\mathcal{R}[\cdot]$ is defined in Table I.

With the derived AND gate inputs $C_{I_1/I_2}(x_1, t)$ in (43) and $C_{P_1/P_2}(x_1, t)$ in (44), the transmitter output $C_O^i(t)$ can be expressed using **Theorem 2** by interchanging the parameters

- in (38) via: $\mathcal{T}[C_{I_{1_0}}(t), 1] \rightarrow C_{I_1/I_2}(x_1, t)$ if an AND gate input is I_1/I_2 , $\mathcal{T}[C_{I_{1_0}}(t), 1] \rightarrow C_{P_1/P_2}(x_1, t)$ if an AND gate input is P_1/P_2 , $n = 2 \rightarrow n = 3$, $H_2(L_{A2}, t) \rightarrow H_3(L_{A2}, t)$;
- in (37) via: $\mathcal{T}[C_N(x_3, t), 4] \rightarrow \mathcal{T}[C_N(x_3, t), 6]$, $C_{Amp_0}(t) \rightarrow C_{Amp_0}^i(t)$, $n = 5 \rightarrow n = 7$.

B. QCSK Receiver

1) *QCSK Receiver Design*: From the communication perspective, the QCSK microfluidic receiver is required to distinguish different concentration levels from different input combinations to achieve demodulation. In this paper, we consider a Gaussian signal $C_O^i(t)$ as the input for the receiver, which can be expressed as

$$C_O^i(t) = \frac{C_{O_0}^i}{\sqrt{2\pi\sigma^2}} e^{-\frac{(t-\mu)^2}{2\sigma^2}} \quad (1 \leq i \leq 4), \quad (45)$$

where the superscript i indicates the four concentration levels of QCSK, μ is the mean, and σ is the standard deviation. For simplicity, we use $C_O(t)$ to denote the general receiver input. The motivation of using Gaussian signal as the receiver input is that it can reveal the dispersion effect of molecule diffusion (i.e., Taylor dispersion) on the transmitted rectangular signals, thus representing the distortion of transmitted signals occurred in the propagation channel between a transmitter and a receiver. For more details on Taylor dispersion, we refer readers to [29]. To focus on the fundamental principle and mechanism of our proposed QCSK transceiver, we leave the analysis of the propagation channel between transmitter

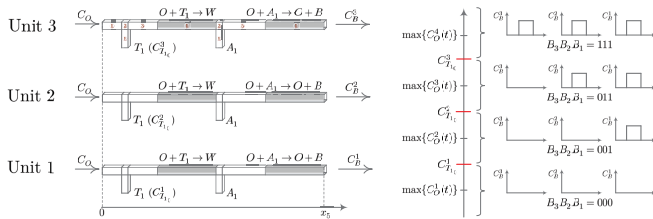


Fig. 9. Three detection units [27] serve as a front-end processing module. Each channel is labeled with a channel number to denote channel length as L_{number} . By setting $\max\{C_O^i(t)\} < C_{T_{10}}^i < \max\{C_O^{i+1}(t)\}$, the front-end processing module can distinguish four concentration regions.

TABLE II

THE RELATION BETWEEN THE RECEIVER INPUT $C_O(t)$, FRONT-END MODULE OUTPUT BINARY SIGNAL B , AND RECEIVER OUTPUT BINARY SIGNAL Y .

$\max\{C_O(t)\}$	B_3	B_2	B_1	Y_2	Y_1
$[0, C_{T_{10}}^1]$	0	0	0	0	0
$[C_{T_{10}}^1, C_{T_{10}}^2]$	0	0	1	0	1
$[C_{T_{10}}^2, C_{T_{10}}^3]$	0	1	1	1	0
$[C_{T_{10}}^3, \infty)$	1	1	1	1	1

and receiver for our future work. We also denote $C_{Y_1}(t)$ and $C_{Y_2}(t)$ as the final demodulated concentration signals, which correspond to the transmitter concentration inputs $C_{I_{10}}(t)$ and $C_{I_{20}}(t)$, respectively.

To detect four concentration levels, we first design three detection units in Fig. 9 to serve as a front-end processing module for the QCSK receiver. Each detection unit follows the receiver design in our initial work [27] and is capable of generating a rectangular signal if the maximum concentration of a received signal exceeds a predefined threshold. As shown in Fig. 9, the only difference among three detection units is the injected concentration $C_{T_{10}}^i(t) = C_{T_{10}}^i u(t)$ ($1 \leq i \leq 3$) of thresholding reactant T_1 . By setting $\max\{C_O^i(t)\} < C_{T_{10}}^i < \max\{C_O^{i+1}(t)\}$, the concentration region of $C_O(t)$ can be identified for three-bit binary signals $B_3B_2B_1$ as shown in Fig. 9. For instance, if $\max\{C_O(t)\} > C_{T_{10}}^3$, all detection units will produce a HIGH state with $B_3B_2B_1 = 111$.

The three detection units in Fig. 9 can only demodulate $C_O(t)$ to three concentration signals $C_B^3(t)$, $C_B^2(t)$, and $C_B^1(t)$ instead of $C_{Y_2}(t)$ and $C_{Y_1}(t)$, which means extra signal processing units are required. Consider the output of front-end module $C_B(t)$ exhibits a rectangular concentration profile and its digital characteristic is ideal to perform logic computations [19], this motivates us to design logic circuits to transform $C_B^i(t)$ to desired outputs $C_{Y_2}(t)$ and $C_{Y_1}(t)$. To inspire the design for this signal transformation, we present the relation between the binary signal B_i ($1 \leq i \leq 3$) and the binary signal Y_j ($j = 1, 2$) in the truth table of Table II. Based on Table II, we express the Boolean equations [38] for Y_2 and Y_1 as

$$Y_2 = \bar{B}_3B_2B_1 + B_3B_2B_1 = B_2B_1, \quad (46)$$

$$\text{and } Y_1 = \bar{B}_3\bar{B}_2B_1 + B_3B_2B_1 = B_1(B_3 \odot B_2), \quad (47)$$

where \bar{B}_3 is the complementary form of B_3 , B_2B_1 represents the AND operation of B_2 and B_1 , and \odot is the Exclusive NOR (XNOR) operation. Inspired by (46) and (47), we connect the front-end module with an AND gate to compute $C_{Y_2}(t)$ as

shown in Fig 10(a), as well as an XNOR gate and an AND gate to calculate $C_{Y_1}(t)$ as shown in Fig. 10(b).

Fig. 10 also includes the splitter that acts as a channel-receiver interface. This interface only has an impact on the velocities of flows entering the front-end processing module, which can be revealed by (12) in Lemma 3. Since the design principle of the QCSK receiver and the mechanisms of all the involved digital gates are independent of the flow velocities, we will not consider the channel-receiver interface in the following analysis.

2) *QCSK Receiver Analysis*: To theoretically characterize receiver outputs $C_{Y_2}(t)$ and $C_{Y_1}(t)$, we denote $C_{[\cdot]_0}(t)$ as the concentration of any injected species $[\cdot]$, and L_i as the length of the microfluidic channel with number i . Moreover, we assume that the injection velocity of any flow is v_{eff} . In the following, we first derive the front-end processing output $C_B^i(t)$ in Fig. 9, and then derive the QCSK receiver outputs $C_{Y_2}(t)$ and $C_{Y_1}(t)$ in Fig. 10. In addition, the **location** and **channel number** are in bold in the following so that readers can easily follow our derivation.

$C_B^i(t)$ Derivation: As shown in Fig. 9, each detection unit in the front-end processing module consists of a thresholding reaction $O + T_1 \rightarrow W$ and an amplifying reaction $O + A_1 \rightarrow O + B$. The output of a detection unit can be expressed using the operator $\mathcal{F}[\cdot]$ defined in Table I as

$$C_B^i(x_5, t) = \mathcal{F}\{\mathcal{T}[C_O(t), 1], \mathcal{T}[C_{T_{10}}^i(t), 1], \mathcal{T}[C_{A_{10}}(t), 1], 2\}, \quad (48)$$

where $C_O(t)$ is the receiver input concentration.

$C_{Y_2}(t)$ Derivation: As shown in Fig. 10(a), $C_B^2(t)$ and $C_B^1(t)$ flow into an AND gate to produce $C_{Y_2}(t)$. At $x = x_6$, $C_{Y_2}(t)$ can be derived as

$$C_{Y_2}(x_6, t) = \mathcal{F}\{\mathcal{T}[\frac{1}{2} \sum_{j=1}^2 C_B^j(x_5, t) * H_3(\frac{2L_2 + L_6 + h}{2}, t), 6], \mathcal{T}[C_{T_{20}}(t), 1], \mathcal{T}[C_{A_{20}}(t), 1], 7\}, \quad (49)$$

where $1/2$ represents the dilution of $C_B^1(x_5, t)$ by $C_B^2(x_5, t)$ and vice versa, $H_n(x, t)$ is given in Theorem 1 with n indicating that the average velocity is nv_{eff} , and the operator $\mathcal{T}[\cdot]$ is defined in Table I.

$C_{Y_1}(t)$ Derivation: As shown in Fig. 10(b), an XNOR gate and an AND gate are linked to the front-end processing module to produce $C_{Y_1}(t)$.

- **XNOR Gate Analysis**: Relying on the fluid separation analysis in Lemma 3, at $x = x_5$, $C_B^j(x_5, t)$ ($j = 2, 3$) is equally separated from channel 9 to channels 10 due to the symmetrical microfluidic design from x_5 to x_9 in Fig. 10(b), resulting in a velocity reduction from $3v_{\text{eff}}$ in channel 4⁵ with $O + A_1 \rightarrow O + B$ to $1.5v_{\text{eff}}$ in channels 10. In channels 11, the confluence of $C_B^3(x_5, t)$ and $C_B^2(x_5, t)$ occurs, and then is diluted by species T_3 injected at x_7 . Subsequently, the outer fluid performs

⁵Since there are three inlets in each unit of the front-end processing module and a flow at each inlet is injected with v_{eff} , the average velocity in channel 4 is $3v_{\text{eff}}$.

$$\begin{aligned}
& C_{R_1}(x_9, t) \\
&= \mathcal{A} \left\{ \underbrace{\mathcal{T} \left[\frac{1}{2} \sum_{j=2}^3 C_B^j(x_5, t) * H_{1.5} \left(\frac{3L_2 + L_9 + 2L_{10} + L_{11} + h + 2w}{2}, t, 3 \right) * \frac{3}{4} H_4(L_2 + L_{12} + L_4, t), \mathcal{T}[C_{A_{3_0}}(t), 1], 5 \right]}_{C_B^{\text{Inner}}(x_7, t)} \right\} \\
&\quad \underbrace{\hspace{10em}}_{C_B^{\text{Inner}}(x_8, t)} \\
& C_{R_2}(x_9, t) = \mathcal{F} \left\{ \underbrace{\mathcal{T} \left[\frac{1}{2} \sum_{j=2}^3 C_B^j(x_5, t) * H_{1.5} \left(\frac{3L_2 + L_9 + 2L_{10} + L_{11} + h + 2w}{2}, t, 3 \right), \mathcal{T}[C_{T_{3_0}}(t), 1], \mathcal{T}[C_{A_{4_0}}(t), 1], 4 \right]}_{C_B^{\text{Outer}}(x_7, t)} \right\}.
\end{aligned} \tag{50}$$

$$\tag{51}$$

In practice, we can deal with this synchronization issue by grouping syringe pumps with a microcontroller board (e.g., Arduino) and sending the release signal to syringe pumps at the same time. For the second case, one example is the synchronization of the two inputs (i.e., $C_{NOT}^1(x_{11}, t)$ and $C_{NOT}^{2\&3}(x_{11}, t)$) of the AND gate used in Fig. 10(b). The synchronization of $C_{NOT}^1(x_{11}, t)$ and $C_{NOT}^{2\&3}(x_{11}, t)$ requires that $C_{NOT}^1(x_{11}, t)$ and $C_{NOT}^{2\&3}(x_{11}, t)$ should arrive at x_{11} simultaneously, which can be achieved by ensuring the inputs $C_O(t)$ of three detection units have the same traveling time from the front-end module to position x_{11} in Fig. 10(b). Based on the fact that the convection effect is merely a shift of the molecular profile in time with average velocity and without any change of shape [39], the design should satisfy the following requirement

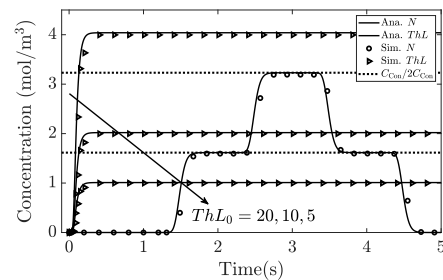
$$\sum_{i \in \mathcal{I}} L_i / v_i = \sum_{j \in \mathcal{J}} L_j / v_j, \tag{56}$$

where \mathcal{I} is the set of the microfluidic channels used to generate $C_{NOT}^{2\&3}(x_{11}, t)$, \mathcal{J} is the set of the microfluidic channels used to generate $C_{NOT}^1(x_{11}, t)$, and L_i and v_i are the channel length and the corresponding flow velocity of microfluidic channel with label i .

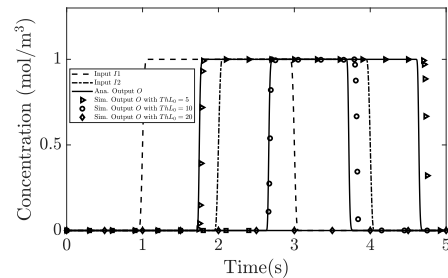
V. PERFORMANCE EVALUATION

In this section, we implement our proposed microfluidic AND gate, QCSK transmitter, and QCSK receiver design⁷ in Fig. 3, Fig. 8, and Fig. 10 using COMSOL Multiphysics, which are then used to validate our corresponding theoretical analysis. The impulse response $H(x, t)$ given in **Theorem 1** is computed in Matlab using *quadgk*. As *quadgk* is only an approximation of $H(x, t)$, the computed results may fluctuate around their steady values. If a computed value is slightly larger than steady value 0, it can induce an instant change on the output value of the indicator function in (30) from 0 to 1, which would further lead to a generation of output signals in undesired regions after an amplifying reaction. To avoid this phenomenon, we modify the statement of an indicator function $C_{S_{i_0}}(t) > 0$ as $C_{S_{i_0}}(t) > \frac{1}{10} \max \{C_{S_{i_0}}(t)\}$. By doing so,

⁷The proposed transceiver is a proof-of-concept design for performing QCSK modulation-demodulation function in molecular domain, and the corresponding testbed will be used for *in vitro* experiments. A discussion about design implementation can be found in our work [27].



(a) The concentration of species N and ThL at $x = x_4$.



(b) The normalized concentrations of input species I_1 , I_2 , and output species O .

Fig. 11. The evaluation of an AND logic gate.

the width of a rectangular output is expected to be smaller than that of the corresponding simulation result. In COMSOL simulations, unless otherwise stated, we set $v_{\text{eff}} = 0.1 \text{ cm/s}$, $D = 10^{-8} \text{ m}^2/\text{s}$, $w = 20 \mu\text{m}$, $h = 10 \mu\text{m}$, $k = 400 \text{ m}^3/(\text{mol}\cdot\text{s})$. Consider these values and water as solvent, the value of the Reynolds number is roughly 3, which is less than 2000 so that the laminar flow assumption is valid. Furthermore, we use “Ana.” and “Sim.” to abbreviate “Analytical” and “Simulation” in all figures.

A. AND Logic Gate

Fig. 11 presents the COMSOL simulation results of the AND logic gate design depicted in Fig. 3. We set the parameters: $C_{I_{1_0}}(t) = 8[u(t-1) - u(t-3)]$, $C_{I_{2_0}}(t) = 8[u(t-2) - u(t-4)]$, $C_{M_0}(t) = 8u(t)$, $C_{Amp_0}(t) = 12u(t)$, $L_T = 80 \mu\text{m}$, $L_C = 20 \mu\text{m}$, $L_R = 500 \mu\text{m}$, $L_{A_2} = 120 \mu\text{m}$. In order to examine the impact of the injected concentration of species ThL on the gate behavior, we consider three cases: $C_{ThL_0}(t) = 5u(t)$, $C_{ThL_0}(t) = 10u(t)$, $C_{ThL_0}(t) = 20u(t)$,

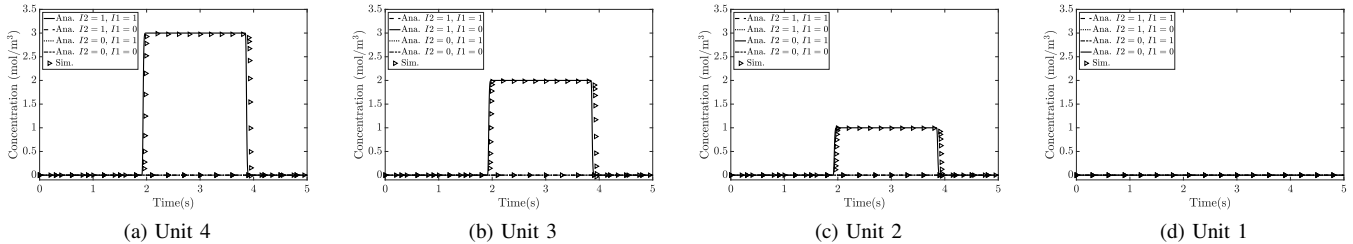


Fig. 12. The output concentrations of the proposed microfluidic QCSK transmitter.

which correspond to the cases $C_{ThL} < C_1$, $C_1 < C_{ThL} < 2C_1$, and $C_{ThL} < 2C_1$ in Fig. 6, respectively.

Fig. 11(a) plots the concentrations of species N and ThL before reaction $N + ThL \rightarrow W$ in Fig. 3. We observe that the simulated concentration points agree with the analytical concentration curves, thus demonstrating the correctness of our analysis of convection-diffusion in **Theorem 1** and convection-diffusion-reaction channels in **Lemma 5**. For the three different injected concentrations, species ThL is nearly diluted to one-fifth of its injected concentration due to that species ThL enters the microfluidic device via the fifth inlet, which validates the concentration analysis for fluid mixing in **Lemma 1**. Moreover, we also plot the concentration constraint C_{Con} in (40) for species ThL using black dash lines. For the curves with $C_{ThL_0}(t) = 5u(t)$ and $20u(t)$, these values do not satisfy the concentration constraint in **Lemma 7**; as expected, the microfluidic device fails to achieve the AND function, which is demonstrated in Fig. 11(b). Fig. 11(b) plots the normalized inputs and the final output product O in (37). Only for $C_{ThL_0}(t) = 10u(t)$, the width of species O equals the width where both input species I_1 and I_2 are HIGH, demonstrating the desired behavior of an AND gate. Furthermore, due to the modification of the indicator function set, we can see the width of (37) is smaller than that of the simulation results.

B. QCSK Transmitter

Fig. 12 plots the outputs of the proposed microfluidic QCSK transmitter design in Fig. 8 and their analytical values $C_O^i(t)$ in Sec. IV-A2. Species I_1 and I_2 are injected with either $12[u(t-1) - u(t-3)]$ representing bit 1 or $0u(t)$ representing bit 0. For other molecular types, their injected concentrations are set as: $C_{P_{10}}(t) = C_{P_{20}}(t) = 12[u(t-1) - u(t-3)]$, $C_{M_0}(t) = 12u(t)$, $C_{ThL_0}(t) = 16u(t)$, $C_{Amp_0}^4(t) = 24u(t)$, $C_{Amp_0}^3(t) = 16u(t)$, $C_{Amp_0}^2(t) = 8u(t)$, and $C_{Amp_0}^1(t) = 0$. The buffer channels are configured with $L_{B1} = 100\mu\text{m}$, $L_{B2} = 150\mu\text{m}$, $L_{B3} = 350\mu\text{m}$, and $L_{B4} = 400\mu\text{m}$.

As shown in Fig. 12, for any input combination, only one unit outputs a HIGH signal except from the case where both I_1 and I_2 are LOW due to $C_{Amp_0}^1(t) = 0$. In addition, for each unit, it is selected under a specific input combination (e.g., Unit 4 is only selected when both input species I_1 and I_2 are HIGH) so that the outputs for other three input combinations are all in a LOW state and the corresponding curves are completely overlapped. Moreover, the analytical curves always capture the simulation points, which again demonstrates the effectiveness of our theoretical analysis $C_O^i(t)$ in Sec. IV-A2. As species

TABLE III
THE PARAMETERS OF THE QCSK RECEIVER.

Molecular Type	Concentration (mol/m ³)	Molecular Type	Concentration (mol/m ³)
A_1	$9u(t)$	T_2	$14u(t)$
A_2	$24u(t)$	T_3	$7u(t)$
A_3	$20u(t)$	T_4	$37u(t)$
A_4	$20u(t)$	NOT	$22u(t)$
A_5	$51u(t)$	V	$28u(t)$

Amp is supplied with different injected concentrations for each unit, we see that the selected unit reaches different concentration levels, proving that the proposed microfluidic QCSK transmitter successfully modulates input bits to the concentration level of output species O .

C. QCSK Receiver

To evaluate the proposed QCSK receiver design in Fig. 10, we consider Gaussian signals $C_O(t)$ with four peak amplitudes as the receiver input: $C_{O_0}^1 = 0$, $C_{O_0}^2 = 0.85$, $C_{O_0}^3 = 1.7$, and $C_{O_0}^4 = 2.55$, with the mean $\mu = 2$ and standard deviation $\sigma = 0.34$. Accordingly, to distinguish these four concentration levels, the concentration of species T_1 for three units in Fig. 9 are set as: $C_{T_{10}}^3(t) = 2.2u(t)$, $C_{T_{10}}^2(t) = 1.2u(t)$, and $C_{T_{10}}^1(t) = 0.8u(t)$. Other parameters and the geometry are summarized in Table III and IV.

Fig. 13 plots the outputs of the proposed QCSK receiver design in Fig. 10 and the corresponding analytical results of $C_{Y_2}(t)$ in (49) and $C_{Y_1}(t)$ in (55). First, we can see that although simulation curves are not in precise agreement with analytical curves, the close match can still confirm the correctness of the mathematical characterization of $C_{Y_2}(t)$ and $C_{Y_1}(t)$. Second, we observe that the width difference between analytical and simulation curves for C_{Y_1} is larger than that for C_{Y_2} . This is because the modification of the statement of an indicator function results in the width difference in each amplifying reaction, and the more amplifying reactions are utilized to compute C_{Y_1} in Fig. 10(b), the bigger the width difference is. Third, we see that the proposed receiver design can well demodulate the received signal $C_O(t)$ to two outputs C_{Y_2} and C_{Y_1} . Recall that we use non-zero concentration to represent HIGH state (bit-1), and zero concentration to represent LOW state (bit-0). We also observe that the relationship between the maximum concentration of the receiver input $\max\{C_O(t)\}$, the concentration of species T_1 , and binary signals Y_2 and Y_1 is in consistent with the truth table of Table II, which demonstrates the effectiveness of our proposed design.

TABLE IV
THE GEOMETRY OF THE QCSK RECEIVER.

Channel Number	Length (μm)	Channel Number	Length (μm)	Channel Number	Length (μm)	Channel Number	Length (μm)
1	80	6	200	11	180	16	1911
2	20	7	350	12	200	17	50
3	100	8	400	13	250	18	300
4	500	9	170	14	500	19	750
5	150	10	180	15	550	20	800

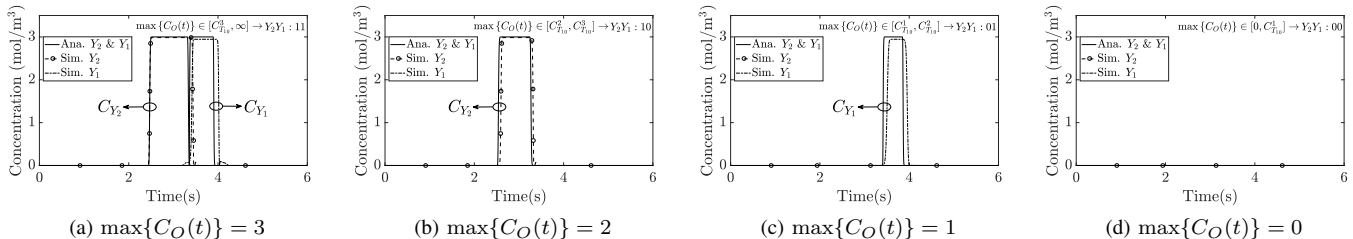


Fig. 13. The output concentrations of the proposed microfluidic QCSK receiver.

VI. CONCLUSION

In this paper, we considered the realization of QCSK modulation and demodulation functionalities for MC using chemical reactions-based microfluidic circuits. We first presented an AND gate design to demonstrate the logic computation capabilities of microfluidic circuits, and then showed how to utilize logic computations to achieve QCSK modulation and demodulation functions. To theoretically characterize a microfluidic circuit, we established a general mathematical framework which is scalable with the increase of circuit scale and can be used to analyze other new and more complicated circuits. We derived the output concentration distributions of the AND gate, QCSK transmitter and receiver designs. Simulation results obtained from COMSOL Multiphysics showed all the proposed microfluidic circuits responded appropriately to input signals, and closely matched our derived analytical results. The QCSK design can be extended to general n th order CSK modulation scheme by using a microfluidic $n : 2^n$ decoder constructed from 2^n AND gates. This extension reveals the scalability and extendibility of our proposed microfluidic circuit design. Thus, we believe that this paper provides not only a design principle and mathematical framework for microfluidic MC circuits, but also a foundation for utilizing simple microfluidic logic gates to produce diverse and complex signal processing functions.

The proposed mathematical framework is a deterministic model and the COMSOL simulation results describe the deterministic responses of our proposed microfluidic circuits. Although COMSOL Multiphysics simulator can simulate flows in the most accurate way, proposing a statistical model for microfluidic circuit to provide more communication insights is an interesting direction for future work. This statistical model can include the noise caused by the mechanical limitations of the solution injections devices (e.g., syringe pump), the noise caused by the chemical reactions, and the noise caused by the external observation equipment (e.g., spectrometer or pH meter). Furthermore, the incorporation of transmitter-channel interface, propagation channel, and the channel-receiver interface into the model makes the model more comprehensive and complete.

APPENDIX A PROOF OF THEOREM 1

To derive the impulse response $H(x, t)$, we formulate the following initial and boundary conditions for (16)

$$C_{S_i}(0, t) = \delta(t), \quad (57a)$$

$$C_{S_i}(x, 0) = 0, \quad x \geq 0, \quad (57b)$$

$$\text{and } \frac{\partial C_{S_i}(x, t)}{\partial x} \Big|_{x=\infty} = 0, \quad t \geq 0, \quad (57c)$$

where $\delta(\cdot)$ is the Kronecker delta function. The Laplace Transform of (16) with respect to t is

$$D_{\text{eff}} \frac{\partial^2 \widetilde{C}_{S_i}(x, s)}{\partial x^2} - v_{\text{eff}} \frac{\partial \widetilde{C}_{S_i}(x, s)}{\partial x} - s \widetilde{C}_{S_i}(x, s) = 0, \quad (58)$$

where $\widetilde{C}_{S_i}(x, s)$ is the Laplace Transform of $C_{S_i}(x, t)$. The general solution for (58) can be expressed as

$$\widetilde{C}_{S_i}(x, s) = d_1 e^{\frac{v_{\text{eff}} + \sqrt{v_{\text{eff}}^2 + 4D_{\text{eff}}s}}{2D_{\text{eff}}} x} + d_2 e^{\frac{v_{\text{eff}} - \sqrt{v_{\text{eff}}^2 + 4D_{\text{eff}}s}}{2D_{\text{eff}}} x}, \quad (59)$$

where d_1 and d_2 are two constants. To determine d_1 and d_2 , we also apply Laplace Transform to (57a) and (57c), which are

$$\widetilde{C}_{S_i}(0, s) = 1, \quad (60)$$

$$\frac{\partial \widetilde{C}_{S_i}(x, s)}{\partial x} \Big|_{x=\infty} = 0. \quad (61)$$

Constrained by these two conditions, we arrive at the particular solution for (58) as

$$\widetilde{C}_{S_i}(x, s) = e^{\frac{v_{\text{eff}} - \sqrt{v_{\text{eff}}^2 + 4D_{\text{eff}}s}}{2D_{\text{eff}}} x}. \quad (62)$$

In order to obtain the impulse response, we need to calculate the inverse Laplace Transform of (62), i.e., $\mathcal{L}^{-1} \left\{ \widetilde{C}_{S_i}(x, s) \right\}$. In the following, we provide two methods to derive $\mathcal{L}^{-1} \left\{ \widetilde{C}_{S_i}(x, s) \right\}$. The first method relies on the table provided

in [40]. According to [40, eqs. (1.3) and (5.58)], the inverse Laplace Transform⁸ can be derived as

$$\mathcal{L}^{-1} \left\{ \widetilde{C}_{S_i}(x, s) \right\} = \frac{x}{2\sqrt{\pi D_{\text{eff}} t^3}} e^{\frac{v_{\text{eff}} x}{2D_{\text{eff}}} - \frac{v_{\text{eff}}^2 t^2 + x^2}{4D_{\text{eff}} t}}. \quad (63)$$

However, when we consider a much more practical scenario, e.g., a time-varying distribution of average velocity due to the imperfectness of syringe pumps, the first method may become infeasible. Therefore, the second method is more general. This method resorts to the Gil-Pelaez theorem and regards $\mathcal{L}^{-1} \left\{ \widetilde{C}_{S_i}(x, s) \right\}$ as a probability density function whose characteristic function⁹ is $\widetilde{C}_{S_i}(x, \omega)$. The cumulative distribution function (CDF) for $\mathcal{L}^{-1} \left\{ \widetilde{C}_{S_i}(x, s) \right\}$ can be expressed as [41]

$$F(x, t) = \frac{1}{2} - \frac{1}{\pi} \int_0^\infty \frac{e^{-j\omega t} \widetilde{C}_{S_i}(x, \omega) - e^{j\omega t} \widetilde{C}_{S_i}(x, \omega)}{2j\omega} d\omega, \quad (64)$$

where $\widetilde{C}_{S_i}(x, \omega)$ is the complex conjugate of $\widetilde{C}_{S_i}(x, \omega)$. Take the derivative of $F(x, t)$ with respect to t , we can arrive at (17).

APPENDIX B

THE DERIVATION OF THE CONCENTRATION OF PRODUCT SPECIES S_k IN (29c)

To derive the concentration of product S_k , we combine (20) and (21) and denote $C(x, t) = C_{S_i}(x, t) + C_{S_k}(x, t)$, which yields

$$\frac{\partial C(x, t)}{\partial t} = D_{\text{eff}} \frac{\partial^2 C(x, t)}{\partial x^2} - v_{\text{eff}} \frac{\partial C(x, t)}{\partial x}. \quad (65)$$

The sum concentration has the following initial and boundary conditions

$$C(0, t) = C_{S_{i_0}}(0, t), \quad (66a)$$

$$C(x, 0) = 0, \quad x \geq 0, \quad (66b)$$

$$\text{and } \left. \frac{\partial C(x, t)}{\partial x} \right|_{x=\infty} = 0, \quad t \geq 0. \quad (66c)$$

As these conditions are the same as (57a)-(57c), we can write

$$C(x, t) = C_{S_{i_0}}(0, t) * H(x, t). \quad (67)$$

Combined with (28a) and (29a), the concentration of product S_k is

$$\begin{aligned} C_{S_k}(x, t) &= C(x, t) - C_{S_i}(x, t) \\ &= \varphi[C_{S_{i_0}}(t), C_{S_{j_0}}(t)] * H(x, t). \end{aligned} \quad (68)$$

⁸In Matlab, we need to manually set value 0 for (63) when $t = 0$ as Matlab returns the scalar “not a number” (NaN).

⁹The Fourier Transform of a probability density function is its characteristic function. The Laplace Transform $\widetilde{C}_{S_i}(x, s)$ can be converted to the corresponding Fourier Transform $\widetilde{C}_{S_i}(x, \omega)$ via $s = j\omega$.

REFERENCES

- [1] D. Bi and Y. Deng, “Microfluidic AND Gate Design for Molecular Communication,” in *Proc. ACM NanoCom*, Sep. 2020, pp. 1–7.
- [2] M. Kuscü *et al.*, “Transmitter and Receiver Architectures for Molecular Communications: A Survey on Physical Design With Modulation, Coding, and Detection Techniques,” *Proc. IEEE*, vol. 107, no. 7, pp. 1302–1341, July 2019.
- [3] V. Jamali *et al.*, “Channel Modeling for Diffusive Molecular Communication—A Tutorial Review,” *Proc. IEEE*, vol. 107, no. 7, pp. 1256–1301, July 2019.
- [4] M. S. Kuran *et al.*, “Modulation Techniques for Communication via Diffusion in Nanonetworks,” in *Proc. IEEE ICC*, June 2011, pp. 1–5.
- [5] B. Koo *et al.*, “Molecular MIMO: From Theory to Prototype,” *IEEE J. Sel. Areas Commun.*, vol. 34, no. 3, pp. 600–614, March 2016.
- [6] H. B. Yilmaz *et al.*, “Three-Dimensional Channel Characteristics for Molecular Communications With an Absorbing Receiver,” *IEEE Commun. Lett.*, vol. 18, no. 6, pp. 929–932, June 2014.
- [7] J. W. Kwak *et al.*, “Two-Way Molecular Communications,” *IEEE Trans. Commun.*, pp. 1–1, 2020.
- [8] Y. Deng *et al.*, “Modeling and Simulation of Molecular Communication Systems With a Reversible Adsorption Receiver,” *IEEE Trans. Mol. Biol. Multi-Scale Commun.*, vol. 1, no. 4, pp. 347–362, December 2015.
- [9] —, “Analyzing Large-Scale Multiuser Molecular Communication via 3-D Stochastic Geometry,” *IEEE Trans. Mol. Biol. Multi-Scale Commun.*, vol. 3, no. 2, pp. 118–133, Jun. 2017.
- [10] A. Noel *et al.*, “Improving Receiver Performance of Diffusive Molecular Communication With Enzymes,” *IEEE Trans. Nanobiosci.*, vol. 13, no. 1, pp. 31–43, March 2014.
- [11] B. Li *et al.*, “CSI-Independent Non-Linear Signal Detection in Molecular Communications,” *IEEE Trans. Signal Process.*, vol. 68, pp. 97–112, Dec. 2019.
- [12] S. Giannoukos *et al.*, “A chemical alphabet for macromolecular communications,” *Anal Chem*, vol. 90, no. 12, pp. 7739–7746, May 2018.
- [13] D. T. McGuinness *et al.*, “Experimental Results on the Open-Air Transmission of Macro-Molecular Communication Using Membrane Inlet Mass Spectrometry,” *IEEE Commun. Lett.*, vol. 22, no. 12, pp. 2567–2570, Dec 2018.
- [14] N. Farsad *et al.*, “Tabletop molecular communication: Text messages through chemical signals,” *PLoS One*, vol. 8, no. 12, p. e82935, December 2013.
- [15] L. Grebenstein *et al.*, “A Molecular Communication Testbed Based on Proton Pumping Bacteria: Methods and Data,” *IEEE Trans. Mol. Biol. Multi-Scale Commun.*, vol. 5, no. 1, pp. 56–62, Oct 2019.
- [16] S. Andresescu and O. A. Sadik, “Trends and Challenges in Biochemical Sensors for Clinical and Environmental Monitoring,” *Pure Appl Chem*, vol. 76, no. 4, pp. 861–878, Jan. 2004.
- [17] B. Alberts *et al.*, “Essential Cell Biology,” (3 ed.). *Garl. Press New York*, 2009.
- [18] B. Wang and M. Buck, “Rapid Engineering of Versatile Molecular Logic Gates using Heterologous Genetic Transcriptional Modules,” *Chem. Commun.*, vol. 50, no. 79, pp. 11 642–11 644, Jul. 2014.
- [19] B. Wang *et al.*, “Engineering modular and orthogonal genetic logic gates for robust digital-like synthetic biology,” *Nat. Commun.*, vol. 2, no. 508, pp. 1–9, Oct. 2011.
- [20] L. J. Kahl and D. Endy, “A Survey of Enabling Technologies in Synthetic Biology,” *J. Biol. Eng.*, vol. 7, no. 1, p. 13, May 2013.
- [21] Y. Xiang *et al.*, “Scaling Up Genetic Circuit Design for Cellular Computing: Advances and Prospects,” *Natural computing*, vol. 17, no. 4, pp. 833–853, Oct. 2018.
- [22] E. Bernard and B. Wang, “Synthetic Cell-based Sensors with Programmed Selectivity and Sensitivity,” in *Biosensors and Biodection*. Springer, Mar. 2017, pp. 349–363.
- [23] A. Tamsir *et al.*, “Robust Multicellular Computing using Genetically Encoded NOR Gates and Chemical ‘Wires’,” *Nature*, vol. 469, no. 7329, pp. 212–215, Jan. 2011.
- [24] T. Ellis *et al.*, “Diversity-based, Model-guided Construction of Synthetic Gene Networks with Predicted Functions,” *Nat Biotechnol.*, vol. 27, no. 5, pp. 465–471, May 2009.
- [25] U. Alon, *An Introduction to Systems Biology: Design Principles of Biological Circuits*. London, UK: Chapman & Hall, 2006.
- [26] Y. Deng *et al.*, “A Microfluidic Feed Forward Loop Pulse Generator for Molecular Communication,” in *Proc. IEEE GLOBECOM*, Dec 2017, pp. 1–7.
- [27] D. Bi *et al.*, “Chemical Reactions-Based Microfluidic Transmitter and Receiver Design for Molecular Communication,” *IEEE Trans. Commun.*, vol. 68, no. 9, pp. 5590–5605, Sep. 2020.

- [28] D. Bi and Y. Deng, "Digital signal processing for molecular communication via chemical-reaction-based microfluidic circuits," *IEEE Commun. Mag.*, vol. 59, no. 5, pp. 26–32, May 2021.
- [29] H. Bruus, *Theoretical microfluidics*. London, UK: Oxford Univ. Press, 2008.
- [30] K. W. Oh *et al.*, "Design of pressure-driven microfluidic networks using electric circuit analogy," *Lab. Chip*, vol. 12, no. 3, pp. 515–545, Nov. 2012.
- [31] D. Scalise and R. Schulman, "Designing Modular Reaction-Diffusion Programs for Complex Pattern Formation," *Technology*, vol. 2, no. 01, pp. 55–66, Mar. 2014.
- [32] A. O. Bicen and I. F. Akyildiz, "End-to-End Propagation Noise and Memory Analysis for Molecular Communication over Microfluidic Channels," *IEEE Trans. Commun.*, vol. 62, no. 7, pp. 2432–2443, July 2014.
- [33] E. De Leo *et al.*, "Communications and switching in microfluidic systems: Pure hydrodynamic control for networking labs-on-a-chip," *IEEE Trans. Commun.*, vol. 61, no. 11, pp. 4663–4677, November 2013.
- [34] M. Kuscu *et al.*, "Graphene-based Nanoscale Molecular Communication Receiver: Fabrication and Microfluidic Analysis," *arXiv:2006.15470*, Jul. 2020.
- [35] R. Chang, *Physical Chemistry for the Biosciences*. Herndon, VA, USA: University Science Books, 2005.
- [36] D. Verrall and W. Read, "A quasi-analytical approach to the advection–diffusion–reaction problem, using operator splitting," *Appl. Math. Model.*, vol. 40, no. 2, pp. 1588–1598, Sep. 2016.
- [37] B. K. Yen *et al.*, "A Microfabricated Gas–Liquid Segmented Flow Reactor for High-Temperature Synthesis: the Case of CdSe Quantum Dots," *Angew. Chem. Int. Ed.*, vol. 44, no. 34, pp. 5447–5451, Aug. 2005.
- [38] D. Harris and S. Harris, *Digital Design and Computer Architecture*. CA, San Mateo: Morgan Kaufmann, 2010.
- [39] W. Hundsdorfer and J. G. Verwer, *Numerical solution of time-dependent advection-diffusion-reaction equations*. New York, NY, USA: Springer, 2013.
- [40] F. Oberhettinger and L. Badii, *Tables of Laplace transforms*. New York, NY, USA: Springer, 1973.
- [41] J. Wendel, "The non-absolute convergence of Gil-Pelaez inversion integral," *The Annals of Mathematical Statistics*, vol. 32, no. 1, pp. 338–339, Apr. 1961.